Contents lists available at ScienceDirect

Biochemistry and Biophysics Reports

Wavelength-dependent photocycle activity of xanthorhodopsin in the visible region

Han-Kuei Chiang, Li-Kang Chu *

Department of Chemistry, National Tsing Hua University, 101, Section 2, Kuang-Fu Rd., Hsinchu 30013, Taiwan

ABSTRACT

Xanthorhodopsin (xR) is a dual-chromophore proton-pump photosynthetic protein comprising one retinal Schiff base and one light-harvesting antenna salinixanthin (SX). The excitation wavelength-dependent transient population of the intermediate M demonstrates that the excitation of the retinal at 570 nm leads to the highest photocycle activity and the excitations of SX at 460 and 430 nm reduce the activity to *ca.* 37% relatively, suggesting an energy transfer pathway from the S_2 state of the SX to the S_1 state of the retinal and a quick internal vibrational relaxation in the S_2 state of SX prior to the energy transfer from SX to retinal.

© 2016 The Authors. Published by Elsevier B.V. This is an open access article under the CC BY-NC-ND license (http://creativecommons.org/licenses/by-nc-nd/4.0/).

1. Introduction

Xanthorhodopsin (xR) is a light-driven proton pump transmembrane protein found in the eubacterium *Salinibacter ruber* [1]. The photochemical process can be initiated not only by the direct photoexcitation of the all-*trans* retinal protonated Schiff base but also by energy transfer from a carotenoid salinixanthin (SX), which is in close proximity to xR, to the retinal [1,2]. The single light-harvesting carotenoid SX makes xR the simplest known antenna system [3], and the absorption of blue photons by SX extends the spectral range of light harvesting [1]. The structure of the protein-carotenoid complex was determined using X-ray diffraction at 1.9-Å resolution. The center-to-center interchromophore distance between SX and the retinal was 11.7 Å, and the angle between the axes of the SX and the retinal was 46° [4]. The experimental results associated with the energy transfer from SX to retinal, including the action spectra for photo-inhibition of the respiration [1,5], the fluorescence and anisotropy studies [6], and femtosecond transient absorption [7,8], revealed a significant energy transfer yield of *ca.* 30–45% [1,5–8]. The energy transfer efficiency was not strongly dependent on the excitation wavelengths in 480–520 nm [6].

The interaction between SX and retinal in xR has been extensively studied using steady-state absorption [7,9,10], fluorescence [6], circular dichroism (CD) [10–12], and a theoretical approach [13]. The absorption features of xR in the visible region are mainly composed of two components, the S_0–S_2 vibronic progressions of the sum of C–C and C=C stretching of the SX at 520, 486, and 458 nm, and the protonated retinal Schiff base at 560 nm [7,9,10,14]. The locked conformation of the SX and retinal in xR leads to the sharpened vibronic features of the SX when the retinal occupied in the binding pocket [9]. Regarding the CD spectrum, the strong optical activity in the visible region includes sharp positive features at 513, 480, and 455 nm and a negative feature at 535 nm, attributed to the SX and the retinal, respectively [12]. Hydrolysis of the retinal Schiff base of xR using hydroxylamine removed the CD characteristics [12]. By replacing the retinal with artificial pigments and changing the pH, Koganov et al. demonstrated that the optical activity can be attributed to an excitonic coupling of the SX and retinal, the SX being located in different subunits of xR, and the chiral conformation of the SX within its binding site [11]. The time-resolved spectroscopic studies manifested the dynamics of the energy transfer between SX and retinal [7,8]. Upon excitation of the SX at 480 nm, the evolution of the associated difference spectra in the near-infrared showed that the instantaneous excitation to the bright state S_2 of the SX not only undergoes internal conversion to the S_1 and S^* states in parallel, within about 100 femtoseconds, followed by the energy cascading to its original state with different rates via the internal conversion, but also transfers the excitation energy to the retinal to induce the isomerization of the retinal [8]. Gdor et al. demonstrated that the energetics of the 0–0 S_0–S_1 transition of the SX is about 12,500 cm^{-1}, which is not energetically sufficient to initiate the photoisomerization of the retinal, which requires 17,500 cm^{-1} [8]. According to experimental results [6–8,15], the energy transfer from the S_2 state of the SX to the S_1 state of the retinal leads to

isomerization of the retinal, without additional routes resulting from the lower excited states of the SX. This energetics schematic was also employed to explain the energy transfer in *Gloeobacter* rhodopsin–salinixanthin complex [16].

Upon excitation of xR at 532 nm, several intermediates in the visible region, similar to those in the bacteriorhodopsin (bR) photocycle [17], were observed [1,18]. The photocycle quantum yield of bR is not dependent on the excitation wavelength in the visible region [19] because the photoexcitation is associated only with the retinal. However, wavelengths of 430–560 nm envelope the excitation of the SX and retinal simultaneously, but few works mentioned the energy transfer efficiency above 480 nm and demonstrated insignificant wavelength dependence [6]. For bR, a transition forbidden $^1A_g^{*-}$ -like π,π^* singlet state exists *ca.* 21,000 cm^{-1} ($\sim$480 nm) above the ground state [20]. Higher electronically excited states were included in the isomerization potential energy surface using time-dependent DFT calculations [21]. Comparison of the sequence in the retinal pocket [22] of xR and bR [4] showed that most of the residues were conserved, and it is reasonable to assume that the retinal in xR has an order of electronic energetics similar to that of bR. As a result, xR could be a good candidate for investigating the energy transfer between the vibronic S_2 states of the SX and higher electronically excited states of the retinal that could potentially lead to the conventional photocycle.

Although previous femtosecond time-resolved works have demonstrated the energy transfer efficiency as 34–40% [7,8] in consistence with other reports [1,5,6], the corresponding excitation wavelength at 480 nm cannot exclude the excitation of retinal. In this present work, the excitation wavelengths were tuned in 430–570 nm, in which the excitation at 430 nm could mostly avoid the excitation of retinal for correctly determining the energy transfer efficiency. By monitoring the transient population of intermediate M at 410 nm in a given period, we are able to estimate the relative photocycle activity at different excitation wavelengths. We therefore provide an alternative approach to obtain the energy transfer efficiencies. We found that as the excitation wavelengths were shortened, the photocycle activity was decreased. The steady-state absorption spectra manifested insignificant photobleaching after pulsed laser excitation. We demonstrated that the decreases in efficiency as the excitation wavelengths were shortened could be attributed to the excitation of the SX instead of the sole excitation of the retinal. The excitation wavelength-independent photocycle activity at 480–430 nm indicated that the same energy transfer process takes place from the S_2 state of the SX to the S_1 state of the retinal.

2. Materials and methods

2.1. Preparation of xanthorhodopsin in DDM micelles

Salinibacter ruber M31 was obtained from the Bioresource Collection and Research Center, Taiwan. The cultivation of *Salinibacter ruber* M31 followed the previous method described by Balashov et al. [1]. The suspension of cell membranes was dialyzed, and the membranes were collected after centrifugation at 40,000*g* for 4 h. The gray pellets of cell tissue were discarded, and the red pellets of membrane fragments containing xR were washed with 0.2 M NaCl and collected. The supernatant was centrifuged again at 40,000*g* for 4 h. The above processes were performed at least 6 times until the supernatant became colorless and transparent. The collected xR membrane fragments were re-suspended by sonicator (Q125, Qsonica) at low power in the presence of 0.2 M NaCl for 15 min. Then dodecylmaltoside (DDM) in 0.01% w/w was
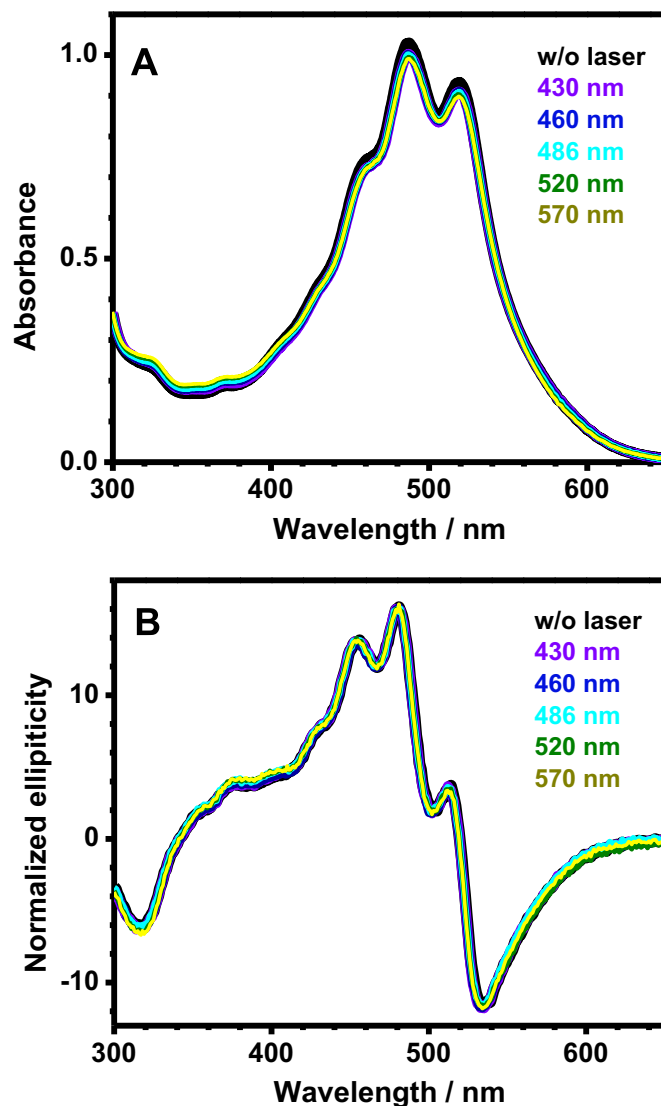
Fig. 1. (A) Steady-state absorption spectra and (B) circular dichroism (CD) spectra of xanthorhodopsin (xR) at pH 9.0 in the presence of 200 mM NaCl before (black line) and after (colored lines) 2-Hz pulsed laser excitations at 570, 520, 486, 460, and 430 nm for 125 min. The incident energy was controlled at 1.5 mJ cm^{-2} for each wavelength.

added to the solution, followed by centrifugation at 40,000*g* for 4 h. Red pellets were collected to remove the unbound salinixanthin. After the extraction with DDM was treated with the above procedure five times, the purification was confirmed by the fact that the absorbance ratio of 280 nm to 568 nm was about 3 [11]. Moreover, xR was identified by sodium dodecyl sulfate polyacrylamide gel electrophoresis (in Fig. S1 in the Supporting Information), steady-state absorption spectrum, and CD spectrum (Fig. 1).

2.2. Spectroscopic measurements

A spectrometer (USB4000-UV-VIS, Ocean Optics) was employed to record the steady-state ultraviolet-visible (UV–Vis) absorption spectra, and a dispersive spectrometer (Model 410, AVIV) was used to collect the circular dichroism (CD) spectra, which were averaged for 10 s at 1-nm intervals at 650–300 nm at 24 °C. Both spectra were recorded before and after the transient absorption experiments. A cuvette with an optical path length of 1 cm was employed in the aforementioned measurements.

Intermediate M at 410 nm served as the detection window to quantify the photocycle activity. The transient absorption module at 410 nm upon excitation in 430–570 nm included a tunable pulsed laser with a simultaneous energy monitor, dispersion monochromator, and a digital oscilloscope for data acquisition. The schematic (Fig. S2) and the description of the experimental setup are supplemented in the Supporting Information.

3. Results & discussions

Steady-state absorption and circular dichroism spectra were collected to confirm the coupling between the salinixanthin and the retinal Schiff base before and after the pulsed excitation. In order to estimate the photocycle activity strength, intermediate M at 410 nm was chosen as the detection window when tuning the excitation wavelengths. Due to the lack of the analytical solution of the temporal behavior of intermediate M, the time-gated population of intermediate M was calculated to derive the relative wavelength-dependent photocycle activity. Then we discussed the difference in the photocycle activity in terms of the energy transfer pathway and energetics.

3.1. Steady-state absorption spectra

The absorption contour of xR before laser excitation is shown in black trace in Fig. 1A. The sharp characteristics of the SX at 520, 486, and 458 nm referred to the locked conformation of the SX bound to protein [9]. After 15,000 pulsed irradiations at 570, 520, 486, 460, and 430 nm with energy flux of 1.5 mJ cm^{-2}, the differences with respect to the unphotolyzed had negligible photo-degradation (less than 4%) and were independent of the excitation wavelengths, as shown in colored traces in Fig. 1A. In addition to the absorption spectra, the circular dichroism spectra were also collected, as shown in Fig. 1B, and the resultant CD contours before and after pulsed laser excitation were almost identical, referring to the negligible decoupling of the retinal and SX due to photobleaching. We therefore confirmed that the transient population of intermediate M upon excitation at different wavelengths in the later sections reflected the wavelength-dependent energy transfer process instead of photobleaching.

3.2. Deriving the photocycle activity

In an analogy with bacteriorhodopsin, the photocycle yield was defined by the extent of the retinal isomerization upon the instantaneous photoexcitation [19,23–25] or the generation of intermediate M [26]. The photocycle quantum yield of bacteriorhodopsin is not dependent on the visible wavelengths [19] because it is only associated with the excitation of the retinal moiety, and the fast internal vibrational relaxation in the excited state of the retinal takes place before the retinal isomerization. However, tuning the wavelengths to 430–570 nm for the excitation of xR is associated with the excitation of the SX and the retinal. As

a result, the photocycle activity will probably change as the excitation wavelengths change, depending on the coupling strengths of the photo-activated vibronic states of the SX and the electronic state of the energy acceptor retinal and the contributions of the SX and retinal in the absorption envelope at the given wavelengths. In this work, the intermediate M served as the indicator for quantifying the relative photocycle activity as the excitation wavelengths were tuned.

When a bunch of laser photons at a given wavelength λ, $n_0(\lambda)$, pass through the xR sample, the number of photons absorbed by xR, $\Delta n(\lambda)$, is equal to the number of excited xR, denoted as xR*, and can be expressed as follows:

$$xR^*(\lambda) = \Delta n(\lambda) = n_0(\lambda) \times \left(1 - 10^{-\text{Abs.}(\lambda)}\right) \quad (1)$$

Abs.(λ) denotes the absorbance of the xR sample at the excitation wavelength λ. Dividing xR*(λ) by the volume (V) that the excitation laser passes through, the concentration of [xR*(λ)] can be determined accordingly. A portion of [xR*(λ)] can undergo retinal isomerization followed by the cascading thermal process to generate the deprotonated retinal Schiff base, i.e., intermediate M, which can be characterized at 410 nm [1,18]. Because the temporal behavior of intermediate M has not been analytically solved due to the complexity of the reaction mechanism, we simplified the temporal profiles as a function of time, f(t), multiplied by a proportional constant including [xR*(λ)] and photocycle efficiency at the excitation wavelength λ, η(λ),

$$[M](\lambda, t) = \eta(\lambda) \times [xR^*(\lambda)] \times f(t) \quad (2)$$

Accounting for the extinction coefficient α for the intermediate M and the absorption path l, the modulation at 410 nm can be expressed using Beer-Lambert's law,

$$\begin{aligned}\Delta\text{Abs.}_{410\,\text{nm}}(\lambda, t) &= \alpha \times l \times [M](\lambda, t) \\ &= \alpha \times l \times \eta(\lambda) \times [xR^*(\lambda)] \times f(t)\end{aligned} \quad (3)$$

Because the intrinsic kinetics of intermediate M is unchanged, that is, the rate coefficients in constructing f(t) are the same, the time-gated population of intermediate M at a given period was derived to account for the relative photocycle activity. The values of the time-gated ΔAbsorbance of intermediate M in 45–1,000 μs $\left(\Delta\text{Abs.}_{410\,\text{nm}}^{\text{gated}}(\lambda)\right)$ were calculated and listed in Table 1. To obtain the photocycle activity via the energy transfer from SX to retinal, the relative η(λ), $\eta_{\text{rel.}}(\lambda)$, with respect to η upon sole excitation of the retinal moiety at 570 nm will be derived for comparison. To rearrange Eq. (3), $\eta_{\text{rel.}}(\lambda)$ can be deduced with the following term,

$$\begin{aligned}\eta_{\text{rel.}}(\lambda) = \frac{\eta(\lambda)}{\eta(570)} &= \frac{\Delta\text{Abs.}_{410\,\text{nm}}^{\text{gated}}(\lambda)}{\Delta\text{Abs.}_{410\,\text{nm}}^{\text{gated}}(570)} \\ &\times \frac{n_0(570) \times \left(1 - 10^{-\text{Abs.}(570)}\right)}{n_0(\lambda) \times \left(1 - 10^{-\text{Abs.}(\lambda)}\right)}\end{aligned} \quad (4)$$

The values of $\eta_{\text{rel.}}(\lambda)$ were summarized in Fig. 4. The observed wavelength dependence will be discussed in Section 3.4.

Table 1
The relative photocycle activity, $\eta_{\text{rel.}}(\lambda)$, at different excitation wavelengths.

|	Excitation wavelength (λ)/nm				
	430	460	486	520	570
$\Delta\text{Abs.}_{410\,\text{nm}}^{\text{gated}}(\lambda)$	73.6 ± 8.2	96.3 ± 10.3	126.3 ± 11.6	158.4 ± 6.4	164.6 ± 3.8
$n_0(\lambda)/10^{15}$ photons cm^{-2}	1.60 ± 0.02	1.70 ± 0.04	1.93 ± 0.01	2.03 ± 0.03	2.08 ± 0.07
Abs.(λ)	0.43	0.74	1.03	0.93	0.22
$\eta_{\text{rel.}}(\lambda)$/%	37 ± 4	35 ± 4	37 ± 3	45 ± 2	100 ± 2

3.3. Excitation power dependence

To prevent the excitation saturation, which could lead to incorrect determination of the photocycle activity, the laser repetition rates and excitation powers were examined. The normalized temporal profiles of the recovery of the xR parent state at 560 nm upon 570 nm excitation at repetition rates of 1, 2, and 5 Hz are shown in Fig. S3 in the Supporting Information. The temporal profile of the recovery at 5 Hz is slightly faster than the other two, implying that the time for recovery after photolysis was insufficient. Accordingly, the excitation repetition rate for the following measurements was set at 2 Hz to avoid overshooting.

The absorption spectrum of xR at 650–430 nm envelops the vibronic features of the retinal and SX. The irradiation at 570 nm excites only the retinal moiety, but the blue-shifted irradiation gradually includes the excitation of the SX and excludes the retinal. Therefore, we have to examine the excitation flux dependences for the SX and the retinal separately because they might exhibit different excitation saturations. The temporal profiles of intermediate M at 410 nm upon 570-nm excitation of the retinal using different excitation fluxes (0.7–2.0 mJ cm^{-2}) are shown in Fig. 2A. The transient population increased as the excitation power was increased. The relationship of the excitation powers and time-gated populations of intermediate M are shown in the inset of Fig. 2A, exhibiting a linearity within the flux of 1.5 mJ cm^{-2}, which was employed to excite xR for obtaining the maximal amplitude without excitation saturation in the further experiments. In the absorption contour of xR in Fig. 1A, the most intense absorption band peaks at 486 nm, implying that the excitation saturation of the SX potentially occurs at 486 nm as the excitation flux is increased. The temporal profiles at 410 nm upon 486-nm excitation with different excitation fluxes (0.7–2.0 mJ cm^{-2}) are shown in Fig. 2B, and the relationships of the excitation fluxes and time-gated M population are shown in the inset, exhibiting a linearity within the flux of 1.5 mJ cm^{-2}. The excitation power will be used in wavelength-scanning experiments to avoid excitation saturation and obtain the maximal signal.

3.4. Photocycle activity upon excitation in 430–570 nm

The temporal profiles of intermediate M upon excitation at different wavelengths are shown in Fig. 3. The resultant time-gated population at 410 nm $\left(\Delta \mathrm{Abs.}_{410\,nm}^{gated}(\lambda)\right)$, incident excitation photons $(n_0(\lambda))$, and absorbance of the sample at the excitation wavelengths $(\mathrm{Abs.}(\lambda))$ are listed in Table 1. The resultant $\eta_{rel.}(\lambda)$ revealed a decrease towards the shorter excitation wavelengths (Fig. 4). Tittor and Oesterhelt demonstrated that the quantum yield of the retinal isomerization of bR is not dependent on the excitation wavelengths at 500–600 nm [27]. Accounting for the absorption contour of xR, the blue-shifted excitation includes more of a contribution from the SX and less of a contribution from the all-trans protonated retinal Schiff base. Most studies have demonstrated that the energy transfer from the S$_2$ state of the SX to the S$_1$ state of the retinal leads to the conventional photocycle [6] with an energy transfer yield of ca. 30–45% [1,5–8]. Upon excitation at 520 nm, $\eta_{rel.}$ begins to decrease because the incident photons are partly used to excite the SX, rather than entirely utilized by the retinal. This change indicates that the energy transfer from SX to retinal is less efficient than the direct excitation of the retinal per photon absorbed, leading to a reduced photocycle activity on average.

For bacteriorhodopsin, the intense absorption at 568 nm is attributed to the transition to the lowest singlet $\pi\pi^*$ $^1B_u^+$ state (S$_1$), which has a large oscillation strength and transition dipole [20].
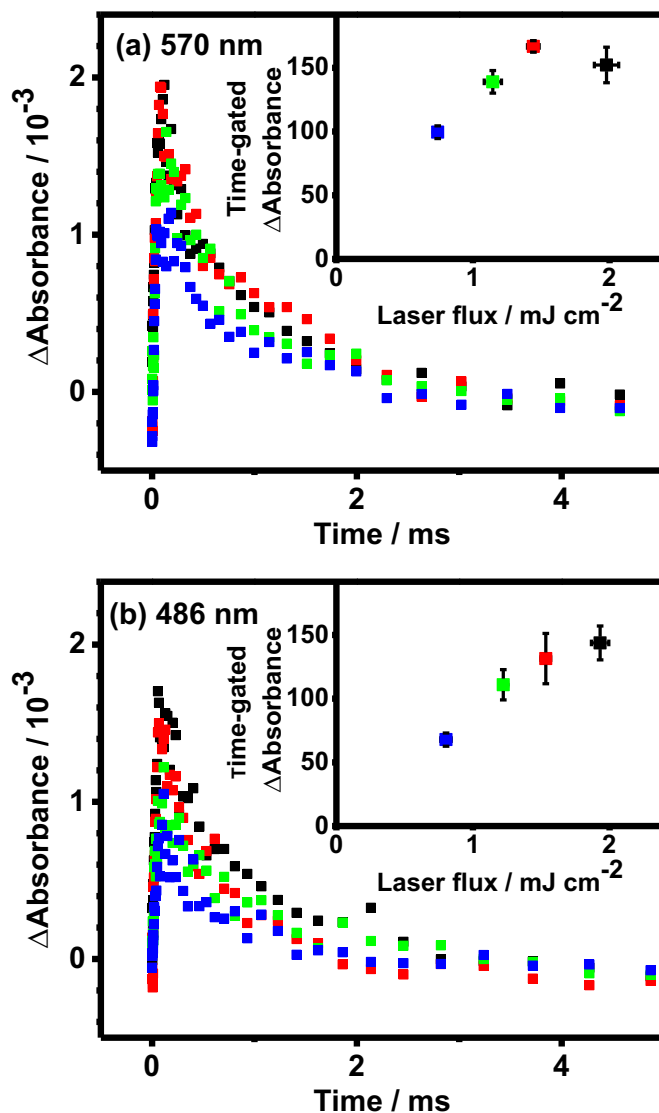
Fig. 2. The temporal profiles at 410 nm upon pulsed excitation of xanthorhodopsin at (A) 570 nm and (B) 486 nm using difference incident flux (0.7–2.0 mJ cm^{-2}). The relationships of the excitation flux and time-gated ΔAbsorbance at 45–1000 μs were shown in the insets. The initial concentrations of xR were made identical by controlling the optical density of 1.0 at 486 nm at pH 9.0 in the presence of 200 mM NaCl and 0.15% DDM.

Two-photon excitation revealed a forbidden state $^1A_g^-$-like lying ca. 21,000–20,500 cm^{-1} above the ground state, roughly equaling 476–487 nm photon energy [20,28]. The S$_2$ state of the retinal was believed to possess the ability to undergo retinal isomerization [29–31], via the jump from the S$_2$ to the S$_1$ state at the avoid-crossing region. If the S$_2$ state of the retinal is prepared by energy transfer from the S$_2$ state of the SX, the $\eta_{rel.}$ will be lower than that from S$_1$ because the S$_2$-to-S$_1$ transition probability of the retinal is determined by the energy gap and the slope of the avoid-crossing potentials interpreted by the Landau-Zener effect and thus could not be 100%. Gdor et al. demonstrated that direct absorption of the retinal at 480 nm is unavoidable in XR and is estimated up to 20% of the absorbed 480 nm photons in the native pigment [8]. In comparison with bR, the retinal absorption in bR below 460 nm is weak, probably implying that the $\lambda_{Ex} < 460$ nm excited majorly the SX moiety in xR with less than 10% excitation of retinal. Our observation showed that the $\eta_{rel.}$ were ca. 37% and the same upon excitation at 430 nm and 460 nm, respectively, suggesting that the
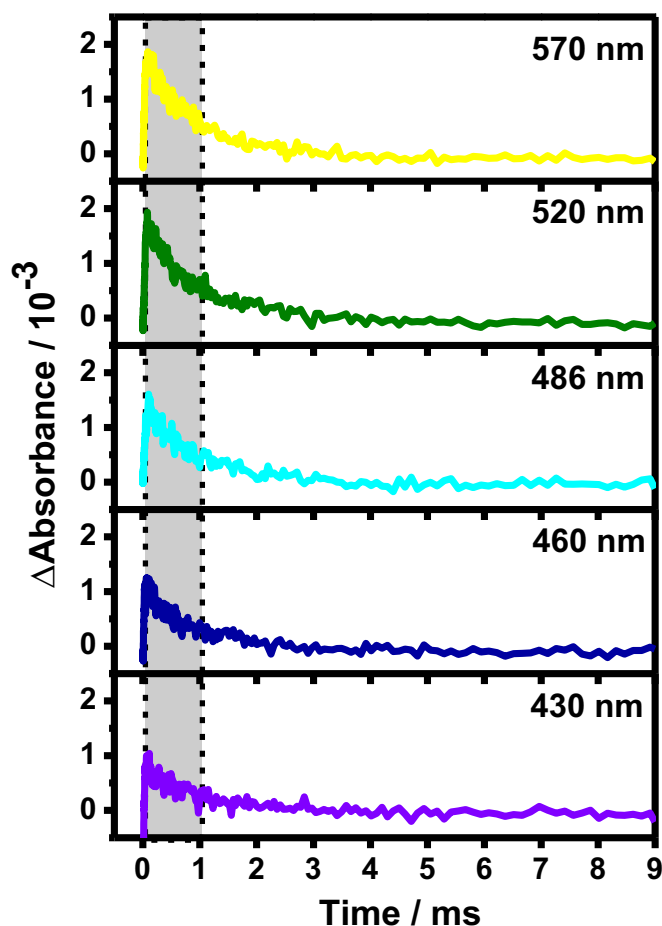
Fig. 3. Temporal profiles at 410 nm upon pulsed photoexcitation at 570, 520, 486, 460, and 430 nm. The colored shadows denote the accumulated period. The fluxes of the excitation pulses were controlled at 1.5 mJ cm^{-2}.
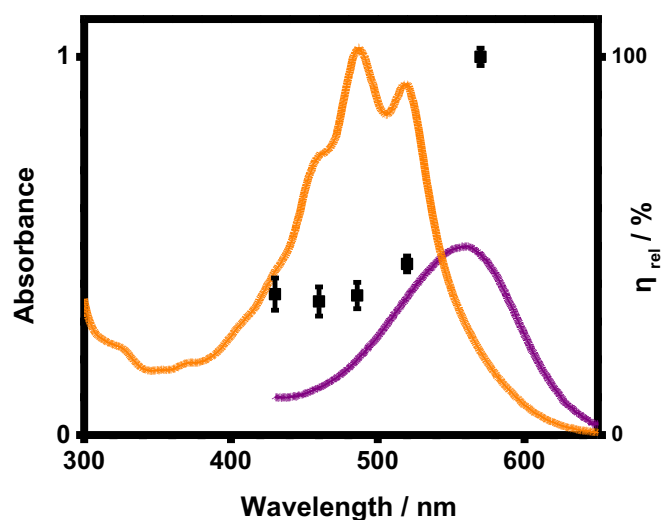

Fig. 4. The relative photocycle activity $\eta_{rel.}$ (squares). The orange and purple lines denote the absorption contour of xR and bR (redshifted by 10 nm) for comparison.

photocycle occurred from the S_1 state of the retinal instead of the S_2, although the energetics allowed for the energy transfer from the S_2 state of the SX to S_2 state of the retinal at 430-nm excitation, according to the analogous energy diagram of bacteriorhodopsin [20,28]. This observation suggests a quick internal vibrational relaxation in the S_2 state of the SX prior to the energy transfer from

the S_2 of the SX to the S_2 of the retinal. It is consistent with the report by Polívka et al. that the lifetime of the S_2 state of the SX (110 fs) is shorter than the time constant of the excitation energy transfer (165 fs) [7].

Acknowledgment

Appendix A. Supplementary material

Supplementary data associated with this article can be found in the online version at http://dx.doi.org/10.1016/j.bbrep.2016.07.009.

Appendix B. Transparency document

Transparency document associated with this article can be found in the online version at http://dx.doi.org/10.1016/j.bbrep.2016.07.009

References

[1] S.P. Balashov, E.S. Imasheva, V.A. Boichenko, J. Antón, J.M. Wang, J.K. Lanyi, Xanthorhodopsin: a proton pump with a light-harvesting carotenoid antenna, Science 309 (2005) 2061–2064.
[2] J.K. Lanyi, S.P. Balashov, Xanthorhodopsin: a bacteriorhodopsin-like proton pump with a carotenoid antenna, Biochim. Biophys. Acta 1777 (2008) 684–688.
[3] V. Šlouf, S.P. Balashov, J.K. Lanyi, T. Pullerits, T. Polívka, Carotenoid response to retinal excitation and photoisomerization dynamics in xanthorhodopsin, Chem. Phys. Lett. 516 (2011) 96–101.
[4] H. Luecke, B. Schobert, J. Stagno, E.S. Imasheva, J.M. Wang, S.P. Balashov, J. K. Lanyi, Crystallographic structure of xanthorhodopsin, the light-driven proton pump with a dual chromophore, Proc. Natl. Acad. Sci. USA 105 (2008) 16561–16565.
[5] V.A. Boichenko, J.M. Wang, J. Antón, J.K. Lanyi, S.P. Balashov, Functions of carotenoids in xanthorhodopsin and archaerhodopsin, from action spectra of photoinhibition of cell respiration, Biochim. Biophys. Acta 1757 (2006) 1649–1656.
[6] S.P. Balashov, E.S. Imasheva, J.M. Wang, J.K. Lanyi, Excitation energy-transfer and the relative orientation of retinal and carotenoid in xanthorhodopsin, Biophys. J. 95 (2008) 2402–2414.
[7] T. Polívka, S.P. Balashov, P. Chábera, E.S. Imasheva, A. Yartsev, V. Sundström, J. K. Lanyi, Femtosecond carotenoid to retinal energy transfer in xanthorhodopsin, Biophys. J. 96 (2009) 2268–2277.
[8] I. Gdor, J. Zhu, B. Loevsky, E. Smolensky, N. Friedman, M. Sheves, S. Ruhman, Investigating excited state dynamics of salinixanthin and xanthorhodopsin in the near-infrared, Phys. Chem. Chem. Phys. 13 (2011) 3782–3787.
[9] E.S. Imasheva, S.P. Balashov, J.M. Wang, E. Smolensky, M. Sheves, J.K. Lanyi, Chromophore interaction in xanthorhodopsin-retinal dependence of salinixanthin binding, Photochem. Photobiol. 84 (2008) 977–984.
[10] E.S. Imasheva, S.P. Balashov, J.M. Wang, J.K. Lanyi, Removal and reconstitution of the carotenoid antenna of xanthorhodopsin, J. Membr. Biol. 239 (2011) 95–104.
[11] E.S. Koganov, V. Brumfeld, N. Friedman, M. Sheves, Origin of circular dichroism of xanthorhodopsin. A study with artificial pigments, J. Phys. Chem. B 119 (2015) 456–464.
[12] S.P. Balashov, E.S. Imasheva, J.K. Lanyi, Induced chirality of the light-harvesting carotenoid salinixanthin and its interaction with the retinal of xanthorhodopsin, Biochemistry 45 (2006) 10998–11004.
[13] K.J. Fujimoto, S. Hayashi, Electronic coulombic coupling of excitation-energy transfer in xanthorhodopsin, J. Am. Chem. Soc. 131 (2009) 14152–14153.
[14] S. Georgakopoulou, R. van Grondelle, G. van der Zwan, Circular dichroism of carotenoids in bacterial light-harvesting complexes: experiments and modeling, Biophys. J. 87 (2004) 3010–3022.
[15] J. Zhu, I. Gdor, E. Smolensky, N. Friedman, M. Sheves, S. Ruhman, Photoselective ultrafast investigation of xanthorhodopsin and its carotenoid antenna salinixanthin, J. Phys. Chem. B 114 (2010) 3038–3045.
[16] E.S.S. Iyer, I. Gdor, T. Eliash, M. Sheves, S. Ruhman, Efficient femtosecond energy transfer from carotenoid to retinal in Gloeobacter rhodopsin–salinixanthin complex, J. Phys. Chem. B 119 (2015) 2345–2349.

[17] R.H. Lozier, R.A. Bogomolni, W. Stoeckenius, Bacteriorhodopsin: a light-driven proton pump in *Halobacterium Halobium*, Biophys. J. 15 (1975) 955–962.

[18] E.S. Imasheva, S.P. Balashov, J.M. Wang, J.K. Lanyi, pH-dependent transition in xanthorhodopsin, Photochem. Photobiol. 82 (2006) 1406–1413.

[19] A. Xie, Quantum efficiencies of bacteriorhodopsin photochemical reactions, Biophys. J. 58 (1990) 1127–1132.

[20] R.R. Birge, C.-F. Zhang, Two-photon double resonance spectroscopy of bacteriorhodopsin. Assignment of the electronic and dipolar properties of the low-lying $^1A_g^{*-}$-like and $^1B_u^{*+}$-like π, π^* states, J. Chem. Phys. 92 (1990) 7178–7195.

[21] H. Tachikawa, T. Iyama, TD-DFT calculations of the potential energy curves for the *trans–cis* photo-isomerization of protonated Schiff base of retinal, J. Photochem. Photobiol. B 76 (2004) 55–60.

[22] R. Henderson, J.M. Baldwin, T.A. Ceska, F. Zemlin, E. Beckmann, K.H. Downing, Model for the structure of bacteriorhodopsin based on high-resolution electron cryo-microscopy, J. Mol. Biol. 213 (1990) 899–929.

[23] H.-J. Polland, M.A. Franz, W. Zinth, W. Kaiser, E. Kölling, D. Oesterhelt, Early picosecond events in the photocycle of bacteriorhodopsin, Biophys. J. 49 (1986) 651–662.

[24] S.L. Logunov, J. Song, M.A. El-Sayed, pH dependence of the rate and quantum yield of the retinal photoisomerization in bacteriorhodopsin, J. Phys. Chem. 98 (1994) 10674–10677.

[25] S.L. Logunov, M.A. El-Sayed, L. Song, J.K. Lanyi, Photoisomerization quantum yield and apparent energy content of the K intermediate in the photocycles of bacteriorhodopsin, its mutants D85N, R82Q, and D212N, and deionized blue bacteriorhodopsin, J. Phys. Chem. 100 (1996) 2391–2398.

[26] B. Becher, T.G. Ebrey, The quantum efficiency for the photochemical conversion of the purple membrane protein, Biophys. J. 17 (1977) 185–191.

[27] J. Tittor, D. Oesterhelt, The quantum yield of bacteriorhodopsin, FEBS 263 (1990) 269–273.

[28] R.R. Birge, Nature of the primary photochemical events in rhodopsin and bacteriorhodopsin, Biochim. Biophys. Acta 1016 (1990) 293–327.

[29] W. Humphrey, H. Lu, I. Logunov, H.-J. Werner, K. Schulten, Three electronic state model of the primary phototransformation of bacteriorhodopsin, Biophys. J. 75 (1998) 1689–1699.

[30] T. Kobayashi, T. Saito, H. Ohtani, Real-time spectroscopy of transition states in bacteriorhodopsin during retinal isomerization, Nature 414 (2001) 531–534.

[31] F. Gai, K.C. Hasson, J.C. McDonald, P.A. Anfinrud, Chemical dynamics in proteins: the photoisomerization of retinal in bacteriorhodopsin, Science 279 (1998) 1886–1891.